

Analyzing and Improving Generative Adversarial Training for Generative Modeling and Out-of-Distribution Detection

Xuwang Yin, Shiyong Li, and Gustavo K. Rohde

University of Virginia, Charlottesville, VA 22904, USA

{xy4cm, sl8jx, gustavo}@virginia.edu

Abstract

Generative adversarial training (GAT) is a recently introduced adversarial defense method. Previous works have focused on empirical evaluations of its application to training robust predictive models. In this paper we focus on theoretical understanding of the GAT method and extending its application to generative modeling and out-of-distribution detection. We analyze the optimal solutions of the maximin formulation employed by the GAT objective, and make a comparative analysis of the minimax formulation employed by GANs. We use theoretical analysis and 2D simulations to understand the convergence property of the training algorithm. Based on these results, we develop an incremental generative training algorithm, and conduct comprehensive evaluations of the algorithm’s application to image generation and adversarial out-of-distribution detection. Our results suggest that generative adversarial training is a promising new direction for the above applications.

1 Introduction

Generative adversarial training (GAT) [61] is a recently introduced defense mechanism for adversarial example detection and robust classification. The defense consists of a committee of detectors (binary discriminators), with each one trained to discriminate natural data of a particular class from adversarial examples perturbed from data of other classes. Like most other work in the area of robust machine learning, the defense is specially designed for defending against norm-constrained adversaries — adversaries that are constrained to perturb the data up to a certain amount as measured by some norm. The defense’s robustness is achieved by training each detector model against adversarial examples produced by the norm-constrained PGD attack [33].

Existing work: training and evaluating robust predictive models A compelling property of the GAT method is that the detector trained with the method exhibits strong interpretability — an unbounded attack that maximizes the detector’s output results in images that resemble the target class data, which suggests the detector has learned the target class data distribution. While the method has been successfully applied to training robust predictive models [61, 58], this behavior of the method is not yet understood at a mathematical, theoretical level.

This work: theoretical understanding, improved training algorithm, and extended applications In order to gain some theoretical understanding of the GAT method, we first analyze the optimal solutions of the training objective (eq. (2)). We start with a *maximin* formulation (eq. (5)) of the objective, and try to connect it with the *minimax* reformulation (eq. (1)) employed in the GANs Framework [13]. We find that the differences between solutions of these two formulations

become immediately clear when we take a game-theory perspective. We then use theoretical analysis and 2D simulations to understand the convergence property of the GAT training algorithm. Building upon these theoretical and experimental insights, we develop an incremental GAT algorithm, and apply it to the tasks of generative modeling and out-of-distribution detection. We find the maximin-based generative model to be more stable to train than its minimax counterpart (GANs), and at the same time more flexible as it does not have a fixed generator and can transform arbitrary inputs to the target distribution data, which might be particularly useful for certain applications (e.g., face manipulation). The model trained with the incremental GAT algorithm also outperforms several state-of-the-art methods on the task of adversarial out-of-distribution detection. In summary, our key contributions are:

- We analyze the optimal solutions of the GAT objective and convergence property of the training algorithm. We discuss the implications of these results on generative modeling and out-of-distribution detection.
- We develop an incremental generative adversarial training algorithm. We conduct a comprehensive evaluation of the algorithm’s application to image generation and adversarial out-of-distribution detection.
- Our comparative analysis of the maximin and minimax problem clarifies misconceptions and provides new insights into how they could be utilized to solve different problems.

2 Related work and background

Generative adversarial networks (GANs) The GANs framework [13] learns a generator function G and a discriminator function D by solving the following *minimax* problem

$$\min_G \max_D V(D, G) = \mathbb{E}_{x \sim p_{\text{data}}} [\log D(x)] + \mathbb{E}_{z \sim p_z} [\log(1 - D(G(z)))]. \quad (1)$$

The generator G implicitly defines a distribution p_g by mapping a prior distribution p_z from a low-dimensional latent space $\mathcal{Z} \subseteq \mathbb{R}^z$ to the high-dimensional data space $\mathcal{X} \subseteq \mathbb{R}^d$. $D : \mathcal{X} \rightarrow [0, 1]$ is a function that discriminates the target data distribution p_{data} from the generated distribution p_g . The minimax problem is solved by alternating between the optimization of D and optimization of G ; under certain conditions, the alternating training procedure converges to a solution where p_g matches p_{data} (Jensen-Shannon divergence is zero), and D outputs $\frac{1}{2}$ on support of p_{data} .

Generative adversarial training (GAT) The GAT method [61] is designed for training adversarial examples detection and robust classification models. In a K class classification problem, the robust detection/classification system consists of K base detectors, with each one trained by minimizing the following objective

$$L(D) = -\mathbb{E}_{x \sim p_k} [\log D(x)] - \mathbb{E}_{x \sim p_{-k}} [\log(1 - \max_{x' \in \mathbb{B}(x, \epsilon)} D(x'))]. \quad (2)$$

In the above objective, p_k is k -th class’s data distribution, p_{-k} is the mixture distribution of all other classes: $p_{-k} = \frac{1}{K-1} \sum_{i=1, \dots, K, i \neq k} p_i$, and $\mathbb{B}(x, \epsilon)$ is a neighborhood of x : $\{x' \in \mathcal{X} : \|x' - x\|_2 \leq \epsilon\}$. The objective is characterized by an *inner maximization* problem and an *outer minimization* problem; when the inner maximization is perfectly solved and D achieves a vanishing loss, D becomes a perfectly robust model capable of separating data p_k , from *any* ϵ -constrained adversarial examples perturbed from data of p_{-k} . A committee of K detectors then provides a complete solution for

detecting any adversarial example perturbed from an arbitrary class. Objective 2 is solved using an alternating gradient method (Algorithm 4), with the first step crafting adversarial examples by solving the inner maximization, and the second step improving the D model on these adversarial examples.

Clearly, the detector’s robustness depends on how well the inner maximization is solved. Despite the fact that D is a highly non-concave function when it is parameterized by a deep neural network, Madry et al. [33] observed that the inner problem could be reasonably solved using projected gradient descent (PGD attack) — a first-order method that employs the following iterative gradient update rule (at initialization $x^0 \leftarrow x$, we consider L^2 -based attack)

$$x^{i+1} \leftarrow \text{Proj}\left(x^i + \gamma \frac{\nabla \log D(x^i)}{\|\nabla \log D(x^i)\|_2}\right), \quad (3)$$

where λ is some step size, and Proj is the operation of projecting onto the feasible set $\mathbb{B}(x, \epsilon)$. The *normalized steepest ascent* rule inside the Proj function, was introduced for dealing with the issue of vanishing gradient when optimizing with the cross-entropy loss [25].

Maximin and minimax problems in game theory In game theory, two-player zero-sum game is a mathematical representation of a situation in which one player’s gain is balanced by another player’s loss. Such a game is described by its *payoff function* $f : \mathbb{R}^{p+q} \rightarrow \mathbb{R}$, which represents the amount of payment that one player (player 1) makes to the other player (player 2). The goal of player 1 is to choose a strategy $u \in \mathbb{R}^p$ such that the payoff is minimized, while the goal of player 2 is to choose a strategy $v \in \mathbb{R}^q$ such that the payoff is maximized. The best strategies for both players, and the resulting payoff, depending on the order of play, could be solved via $\min_u \max_v f(u, v)$ or $\max_v \min_u f(u, v)$.

In the minimax game $\min_u \max_v$, player 1 makes the first move. Player 2, after learning that player 1 has made the move u , will choose a v to maximize $f(u, v)$, which results in a payoff of $\max_v f(u, v)$. Player 1, who is informed of player 2’s strategy, will choose a u such that the worst case payoff $\max_v f(u, v)$ is minimized, which results in a payoff of $\min_u \max_v f(u, v)$.

In the maximin game $\max_v \min_u$, the order of play is reversed. Player 2 makes the first move, and then player 1 minimizes the payoff by choosing $u = \arg \min_u f(u, v)$. Player 2 knows that player 1 will follow this strategy and will choose a v such that the worst case payoff $\min_u f(u, v)$ is maximized, which results in a payoff of $\max_v \min_u f(u, v)$.

The payoff $\min_u \max_v f(u, v)$ is always greater or equal to $\max_v \min_u f(u, v)$. This difference can be intuitively understood as the result of player 2’s extra knowledge gained by taking the second move. According to the minimax theorem [40], when f is a continuous function that is concave-convex (i.e., for each v , $f(u, v)$ is a convex function of u , and for each u , $f(u, v)$ is a concave function of v), these two quantities are equal. We refer the reader to [3] (§5.4.3, §10.3.4) for more details on this topic.

Out-of-distribution detection We provide a review of related work on out-of-distribution detection in Appendix B.

3 Theoretical results

In this section we first reformulate objective 2 into a *maximin* problem, and then analyze the optimal solutions of the maximin problem and convergence property of Algorithm 1. We then discuss the optimal solution of the corresponding *minimax* formulation and the differences between

the solutions of these two formulations. The popular generative modeling approach of GANs learns a data distribution by solving the minimax problem, but there seems to be a misconception about the differences between solutions of these two problems, and as a result, a false impression that the GANs algorithm could solve the maximin problem (Goodfellow [12], §5.1.1). Our analysis of optimal solutions is based on a game-theory interpretation of these problems, and the differences between these solutions are immediately clear under such an analysis.

3.1 The maximin problem

To gain some theoretical understanding of objective 2, it is useful to reformulate the problem. First, maximizing D is equivalent to minimizing $\log(1 - D)$, hence eq. (2) is equivalent to

$$L(D) = -\mathbb{E}_{x \sim p_k} [\log D(x)] - \mathbb{E}_{x \sim p_{-k}} \left[\min_{x' \in \mathbb{B}(x, \epsilon)} \log(1 - D(x')) \right]. \quad (4)$$

We restrict our attention to analyzing the optimal solution of D under the scenario where ϵ is large enough such that perturbations cover the entire data space: $\mathbb{B}(x, \epsilon) = \mathcal{X}$. In this scenario, imposing perturbations on p_{-k} samples can be considered as moving mass of p_{-k} to locations in \mathcal{X} via a transformation function $T : \mathcal{X} \rightarrow \mathcal{X}$. Utilizing the technique of random variable transformation, we can write the density function of the resulting distribution p_t as a function of p_{-k} : $p_t(y) = \int_{\mathcal{X}} p_{-k}(x) \delta(y - T(x)) dx$. Let $\mathcal{M}_+^1(\mathcal{X})$ be the set of distributions obtained by applying such transformations to the support of p_{-k} , the inner problem in eq. (4) could then be interpreted as determining the distribution in $\mathcal{M}_+^1(\mathcal{S})$ that causes the highest (expected) loss of the D function. The interplay of the D model and the adversary can be formulated as a *maximin* problem:

$$\max_D \min_{p_t \in \mathcal{M}_+^1(\mathcal{X})} U(D, p_t) = \mathbb{E}_{x \sim p_k} [\log D(x)] + \mathbb{E}_{x \sim p_t} [\log(1 - D(x))]. \quad (5)$$

A convenient way of analyzing the above problem is to consider it as a two-player zero-sum game: U can be interpreted as the *payoff function* which represents the amount of payment that one player (player p_t) makes to the other player (player D). The goal of player p_t is to choose a strategy $p_t \in \mathcal{M}_+^1(\mathcal{X})$ such that the payoff is minimized, while the goal of player D is to choose a strategy $D \in \mathcal{D}$ such that the payoff is maximized. This *maximin* game is played by following such a rule: player D makes the first move by choosing a D ; player p_t , after learning that player D has made the move, will choose a p_t to minimize its payment, which results in a payoff of $\min_{p_t} U(D, p_t)$; player D , who is informed of player p_t 's strategy, will choose a D such that the worst case payoff $\min_{p_t} U(D, p_t)$ is maximized, which results in an overall payoff of $\max_D \min_{p_t} U(D, p_t)$. Following this rule, we could derive the optimal strategy for player D :

Proposition 1. *In the maximin game $\max_D \min_{p_t} U(D, p_t)$, the best strategy for player D is to choose a D that outputs $\frac{1}{2}$ in $\text{Supp}(p_k)$ and $\leq \frac{1}{2}$ in $\mathcal{X} \setminus \text{Supp}(p_k)$.*

The mathematical derivations of this optimal solution is included in Appendix C. This optimal solution of D can also be verified by assuming a different D value than the claimed one, and show that the payoff player D could receive is always lower than that with the claimed one. In particular, if there is a point $q \in \mathcal{X}$ with $D(q) > \frac{1}{2}$, then player p_t could choose a p_t with *all its mass* concentrated on q , and hence cause a lower payoff (due to the term $\mathbb{E}_{x \sim p_t} [\log(1 - D(x))] |_{x=q}$). On the other hand, if there is a $q \in \text{Supp}(p_k)$ with $D(q) < \frac{1}{2}$, player D 's payoff is also going to be lower because the term $\mathbb{E}_{x \sim p_k} [\log(D(x))]$ has a lower value than the case where D outputs $\frac{1}{2}$ everywhere in $\text{Supp}(p_k)$.

Given player D 's optimal strategy, player p_t 's optimal strategy is to choose a p_t with its mass distributed in locations where D outputs $\frac{1}{2}$.

3.2 The maximin problem solver

While the game-theory interpretation is useful for understanding the problem, the optimal solution of D as predicted by the theory seems not very interesting. We next show that the *actual* D solution, as obtained via a numerical algorithm, has some interesting properties and is useful for a few applications. We start with a “translation” of Algorithm 4 into our maximin language, which results in a solver (Algorithm 1) for the maximin problem.

Algorithm 1 The maximin problem solver

- 1: Initialize parameters of D .
 - 2: Sample minibatch of m samples $\{x_1^k, \dots, x_m^k\}$ from p_k , and m samples $\{x_1^{-k}, \dots, x_m^{-k}\}$ from p_{-k} .
 - 3: Compute perturbed samples $\{x'_1, \dots, x'_m\}$ by solving $\min_{x' \in \mathcal{X}} D(x')$ for each x_i^{-k} .
 - 4: Update D by maximizing $\frac{1}{m} \sum_{i=1}^m [\log D(x_i^k) + \log(1 - D(x'_i))]$ (single step).
 - 5: Return to step 2.
-

We consider the case where D is parameterized by a neural network. The parameters are initialized in step 1 of Algorithm 1, which typically results in a highly non-concave function ([14], §8.2.2). Then in each iteration, step 2 samples points from p_k and p_{-k} , step 3 solves the inner minimization of eq. (5) by moving samples of p_{-k} to locations where D has the maximum outputs (which results in a new distribution p_t), and step 3 solves the outer maximization of eq. (5) by increasing D outputs on p_k samples (maximizing $\mathbb{E}_{x \sim p_k} [\log D(x)]$) and decreasing outputs on p_{-k} samples (maximizing $\mathbb{E}_{x \sim p_t} [\log(1 - D(x))]$).

Step 3 is implemented as a gradient-based search procedure: it uses samples of p_{-k} as starting points, and performs gradient ascent on D (eq. (3)). When D is a highly non-concave function, this process will inevitably get stuck in local maxima. Our 2D simulation of Algorithm 1 indicates that this problem is resolved by the alternating optimization procedure: if at step 3 samples of p_{-k} got stuck at local maxima, step 4 immediately decreases D outputs on these samples. In other words, local maxima are constantly being eliminated during the course of algorithm execution. This pattern can be clearly observed in Figure 7.

Another issue with step 3 is concerned with the distribution of p_{-k} data. As illustrated in Figure 1, when p_{-k} data is concentrated in a subspace in the bottom left corner, Algorithm 1 converged to a D solution with $> \frac{1}{2}$ outputs in locations other than $\text{Supp}(p_k)$. Inspecting the gradient vector field in Figure 1(b), we find that by starting from p_{-k} and following the gradient of D , p_{-k} samples always end up at $\text{Supp}(p_k)$; local maxima points on other locations can not be reached by p_{-k} samples and hence can not be eliminated.

To solve the above issue, we could use a p_{-k} that is distributed in the entire data space, as opposed to one that is concentrated in a small subspace. In the same 2D experiment, when we use a *uniform distribution* in the data space as p_{-k} , in multiple trials of the experiment we consistently obtained D solutions with global maxima at $\text{Supp}(p_k)$ and no local maxima (Figure 1(c) and Figure 8 bottom row).

Convergence of Algorithm 1 Equipped with knowledge gained from the 2D experiment, we now explore the convergence property of Algorithm 1. We assume that optimizing the first term $\mathbb{E}_{x \sim p_k} [\log D(x)]$ of eq. (5) does not affect D 's outputs outside of $\text{Supp}(p_k)$ when D has enough capacity. In the second term $\mathbb{E}_{x \sim p_t} [\log(1 - D(x))]$, p_t is the new distribution formed by taking p_{-k} samples as starting points and performing gradient ascent on D ; for any $q \in \text{Supp}(p_t)$, q is either in $\text{Supp}(p_k)$, or on a local maximum point in $\mathcal{X} \setminus \text{Supp}(p_k)$. Collectively, optimizing this term either causes local maxima values to decrease (when there exists p_t samples located in local

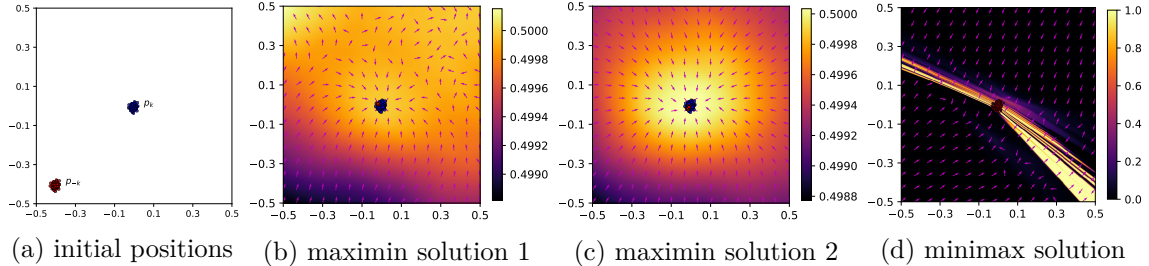


Figure 1: Plots of contours and gradient vector fields of the D functions (gradient vectors are normalized to have the unit length). (a) The initial positions of p_{-k} and p_k . (b) The solution obtained by the maximin problem solver. (c) The solution obtained by the maximin problem solver when p_{-k} is a uniform distribution in the data space. (d) The solution obtained by the minimax problem solver.

maxima points in $\mathcal{X} \setminus \text{Supp}(p_k)$, or does not affect D 's outputs in $\mathcal{X} \setminus \text{Supp}(p_k)$ (when p_t samples are all in $\text{Supp}(p_k)$). This observation leads to a conjecture that if we run Algorithm 1 for enough iterations local maxima in $\mathcal{X} \setminus \text{Supp}(p_k)$ will eventually disappear. We now show that under certain conditions Algorithm 1 has the following convergence property:

Proposition 2. *If D has enough capacity and p_{-k} has non-zero density everywhere in the space $\mathcal{X} \setminus \text{Supp}(p_k)$, then for any initialization of D , Algorithm 1 converges to a D solution with global maxima at $\text{Supp}(p_k)$ and no local maxima; the global maxima value is $\frac{1}{2}$.*

Proof. We first prove that any local maximum in $\mathcal{X} \setminus \text{Supp}(p_k)$ can be eliminated by running Algorithm 1 for a sufficient and finite number of iterations. To proceed, we first state the condition under which a local maximum will be eliminated: a local maximum in $\mathcal{X} \setminus \text{Supp}(p_k)$ will be eliminated if via one or more iterations of the algorithm a sufficient number of p_{-k} samples reach the local maximum point by performing gradient ascent on D (step 3). When this condition is satisfied, the cumulative execution of step 4 cause the local maximum value to decrease to a sufficiently small value and the local maximum to disappear.

We next show that for any local maximum point $q \in \mathcal{X} \setminus \text{Supp}(p_k)$ the above condition is always satisfied when Algorithm 1 runs for a sufficient and finite number of iterations. Let U be a neighborhood of q where q is the only critical point. U is non-empty by definition and any $p \in U$ can reach q via gradient ascent on D when a sufficiently small step size is used. For p_{-k} has non-zero density everywhere, a sufficient number of p_{-k} samples could fall on U and subsequently reach q via gradient ascent if enough samplings of p_{-k} are done via step 1. We note that the definition of U could change after D 's update in step 4, but U is non-empty as long as q is still a local maximum point.

Finally we note that after D 's update in step 4 the set of local maxima in $\mathcal{X} \setminus \text{Supp}(p_k)$ could also change (the number of local maxima points could even increase due to D 's update). But because the integral of D on $\mathcal{X} \setminus \text{Supp}(p_k)$ is a finite value and hence can not be decreased for infinite number of times, the set of local maxima points in $\mathcal{X} \setminus \text{Supp}(p_k)$ will eventually become empty. \square

3.3 The minimax problem

Compared to the maximin game, the minimax game $\min_{p_t} \max_D U(D, p_t)$ has a reversed rule: player p_t makes the first move by choosing a p_t ; player D then chooses a D to maximize its payoff,

Algorithm 2 The minimax problem solver

- 1: Initialize $p_t \leftarrow p_{-k}$.
 - 2: **repeat**
 - 3: Update D by maximizing $\mathbb{E}_{x \sim p_k} [\log D(x)] + \mathbb{E}_{x \sim p_t} [\log(1 - D(x))]$ (until converge).
 - 4: For each $x \in p_t$, update its value by $x \leftarrow x - \lambda \frac{\nabla \log(1 - D(x))}{\|\nabla \log(1 - D(\bar{x}))\|_2}$ (single step).
 - 5: **until** p_t converges to p_k
-

which results in a payoff of $\max_D U(D, p_t)$; player p_t knows player D 's strategy and will choose a p_t such that the worst case payoff $\max_D U(D, p_t)$ is minimized, which results in an overall payoff of $\min_{p_t} \max_D U(D, p_t)$.

The solution of this minimax game is analyzed in [13, 12]: the optimal strategy of player p_t is to choose a p_t that minimizes the Jensen-Shannon divergence (JSD) between p_t and p_k : $p_t^* = \arg \min_{p_t \in \mathcal{M}_+^1(\mathcal{X})} \text{JSD}(p_t \parallel p_k) = p_k$, and the optimal strategy of player D is to choose $D^* = \frac{p_k}{p_k + p_t} = \frac{1}{2}$. Under these strategies, the payoff function U measures the JSD between p_t and p_k : $U(D^*, p_t^*) = -\log(4) + 2 \cdot \text{JSD}(p_t^* \parallel p_k) = -\log(4)$. It should be noted that D^* does not need to be defined outside of $\text{Supp}(p_t) \cup \text{Supp}(p_k)$ [13].

Removing the “generator” from GANs’ training algorithm ([13] §4) gives us a solver (Algorithm 2) for the minimax problem. According to [13], if at each step p_t is updated with a sufficiently small step of λ , and D is trained to reach its optimum, then p_t converges to p_k . 2D simulation results in Figure 1(d) and Figure 9 confirm this convergence property.

3.4 The difference

There are a few differences between the solutions of the maximin problem and minimax problem.

D solution difference While both D^* s output $\frac{1}{2}$ in $\text{Supp}(p_k)$, their outputs outside of $\text{Supp}(p_k)$ are different. In the maximin problem, the ideal D solution outputs $< \frac{1}{2}$ and has no local maxima outside of $\text{Supp}(p_k)$. In contrast, D^* in the minimax game does not need to be defined outside of $\text{Supp}(p_k)$. In other words, D^* in the minimax problem has unpredictable behavior outside $\text{Supp}(p_k)$. This phenomenon can be observed in Figure 1(d) and Figure 9. This difference has an intuitive explanation from the game-theory perspective: in the maximin game, p_t^* is decided in the second move, with the knowledge of the current D value; to prevent player p_t from taking this advantage, the best strategy for player D is to specify D outputs for the entire data space. In the minimax game, on the contrary, D^* is decided in the second move, with the knowledge of p_t , hence player D does not need to be concerned with D^* outputs on locations other than supports of p_t and p_k .

p_t solution difference Another difference, which can also be observed from Figure 1, is that in the minimax game, p_t^* exactly matches p_k , while in the maximin game, mass of p_t^* can be any location where D^* outputs $\frac{1}{2}$.

Overall we find these two formulations giving rise to different applications. The minimax formulation, which is the formulation used by GANs, is perfect for learning a generator that produces a distribution that exactly matches the target data distribution. The discriminator (the D model), because of its undefined behavior in most of the data space, may not be very useful for downstream tasks. The maximin problem, if well solved (Figure 1(c)), gives a D function that models a *characteristic function* of the data distribution, and could be used to solve problems that require this feature (Section 4).

4 Implementation and Applications

Applications Continuing our discussion from Section 3.2, when p_{-k} has non-zero density everywhere in the space $\mathcal{X} \setminus \text{Supp}(p_k)$, the maximin problem solver gives us a D function with global maxima at the $\text{Supp}(p_k)$ and no local maxima. We think this function is at least useful for the following two applications:

- **Out-of-distribution (OOD) detection** Because D outputs $< \frac{1}{2}$ for any data that is outside of $\text{Supp}(p_k)$, we can use D outputs to identify out-of-distribution inputs.
- **Generative modeling** We can transform an arbitrary out-of-distribution sample into a target distribution (p_k) sample by taking the sample as the starting point and performing gradient ascent on D , until the sample reaches support of the target distribution.

We note that this new generative modeling technique differs from standard approaches in that it does not learn a fixed “generator”. This feature may facilitate certain generation tasks as demonstrated in Figure 2, 3, 4 and 5.

p_{-k} data While the 2D simulation results suggest uniform distribution be an ideal candidate for p_{-k} , we find uniform noise to be ineffective when training in high-dimensional space (Appendix E.2). Our interpretation of these results is that real image samples lie on low-dimensional manifolds embedded within the high-dimensional space, and are close to each other in terms of geodesic distance ([14], §5.11.3). Uniform noise, on the other hand, is distributed in the entire space and may require substantially much larger perturbations and hence training time in order to reach a satisfactory performance. This observation leads us to consider using a large, diverse, real image dataset, as the p_{-k} dataset.

Incremental training algorithm Another issue with Algorithm 1 is the implementation of Step 3. As a gradient-based search procedure (Section 3.2), Step 3 needs the step size and the number of steps to be specified. Regarding the step size, a sufficiently small value should be used in order for Step 4 to converge to local maxima (see the ablation study in Appendix F). Setting an appropriate value for the number of steps poses a challenge: the number of steps should be large enough such that the search covers enough data space, but this will incur a very high computational cost (evaluating $\nabla_x D(x)$ requires running a full forward-backward pass on the neural network that parameterizes D). On the other hand, performing more steps of gradient ascent is meaningless and a waste of computation once the search got stuck in local maxima.

These challenges motivate us to consider an incremental training scheme — we could gradually increase the search radius by using an increasing sequence of number of steps, which is equally effective for locating local maxima but much more computationally efficient. We implement this incremental training idea in Algorithm 3: in the outer loop, we use an increasing sequence of number of steps (K); in the inner loop, due to the steepest descent update rule (Line 4; note there is no **Proj** operation here), the search radius is always $\leq \lambda K$; as we increase K , the search radius of the algorithm increases. In practice we find that this incremental algorithm indeed trains faster, and at the same time converges faster (Appendix E.1).

The incremental training algorithm also provides a mechanism for mitigating overfitting. Overfitting could happen in our approach because the algorithm learns a characteristic function that outputs $\frac{1}{2}$ on $\text{Supp}(p_k)$ and $< \frac{1}{2}$ outside of $\text{Supp}(p_k)$; when p_k is an empirical distribution, the $\frac{1}{2}$ outputs are at p_k ’s samples. In that case, gradient ascent on D converges to p_k ’s samples. However, this only happens when the search covers $\text{Supp}(p_k)$ (Line 3 of Algorithm 1). In Algorithm 3, by controlling K and hence the search radius, we could mitigate overfitting and learn a D function

that captures the manifold structure of the p_k data. Overfitting could also be mitigated by properly constraining the step size and number of steps when performing gradient ascent on D .

Algorithm 3 Incremental Generative Adversarial Training

- 1: **for** K in $[0, 1, \dots, N]$ **do**
 - 2: **for** number of training iterations **do**
 - 3: Sample minibatch m samples $\{x_1, \dots, x_m\}$ from p_k , and m samples $\{\tilde{x}_1, \dots, \tilde{x}_m\}$ from p_{-k} .
 - 4: For each sample \tilde{x}_i in $\{\tilde{x}_1, \dots, \tilde{x}_m\}$, compute the perturbed sample \tilde{x}_i^K by performing K steps normalized steepest descent $\tilde{x}_i^{k+1} \leftarrow \tilde{x}_i^k - \gamma \frac{\nabla \log(1-D(\tilde{x}_i^k))}{\|\nabla \log(1-D(\tilde{x}_i^k))\|_2}$ (at initialization $\tilde{x}_i^0 \leftarrow \tilde{x}_i$).
 - 5: Update D by maximizing $\frac{1}{m} \sum_{i=1}^m [\log D(x_i) + \log(1 - D(\tilde{x}_i^K))]$ (single step).
 - 6: **end for**
 - 7: **end for**
-

5 Experiments

5.1 OOD detection

We evaluate our method’s application to out-of-distribution detection on CIFAR-10 [27] and SVHN [39] dataset. In these two tasks, we respectively use CIFAR-10 and SVHN as the p_k dataset, and use the 800 Million Tiny Images dataset [57] as the p_{-k} dataset (same as [2]). We use the standard ResNet18 architecture as the D model and Algorithm 3 to train the models. Area under the receiver operating characteristic curve (AUROC) is used as the performance metric.

Table 1 and Table 2 report adversarial OOD detection performances of our method and several state-of-the-art methods (performance data of these methods is collected from [2]). It is observed that adversarial perturbations cause significant performances decrease of non-robust models (OE and our method with $K = 0$). (Performances on the standard OOD detection task are reported in Table 8.) Our method trained with $K = 5$ (CIFAR-10) and $K = 45$ (SVHN) outperforms several state-of-the-art methods in some entries.

Table 1: CIFAR-10 adversarial OOD detection performances (AUROC scores). The results of our method are based on an PGD attack of steps 100 and step size 0.002. For results under different attack configurations including one with random restarts see Table 6.

Method	OOD dataset (with an L^∞ perturbation of $\epsilon = 0.01$)			
	Uniform Noise	Gaussian Noise	SVHN	CIFAR-100
OE [17]	75.7	N/A	3.7	11.0
CCU [36]	100	N/A	14.8	23.3
ACET [15]	98.9	N/A	88.0	74.5
GOOD [2]	99.5	N/A	58.9	54.7
Ours ($K = 0$)	97.8	22	1.0	7.1
Ours ($K = 5$)	99.0	99.1	91.8	81.8

5.2 Image generation

We evaluate our method’s application to image generation on CelebA-HQ [20], LSUN-BEDROOM [62], and the ImageNet-Dog dataset [59]. In these tasks, we respectively use the above three datasets

Table 2: SVHN adversarial OOD detection performances (AUROC scores). The results of our method are based on an PGD attack of steps 100 and step size 0.005. For results under different attack configurations including one with random restarts see Table 7.

Method	OOD dataset (with an L^∞ perturbation of $\epsilon = 0.03$)			
	Uniform Noise	Gaussian Noise	CIFAR-10	CIFAR-100
OE [17]	98.2	N/A	62.5	60.2
CCU [36]	100	N/A	56.8	52.5
ACET [15]	96.3	N/A	99.5	99.4
GOOD [2]	99.9	N/A	98.4	97.7
Ours ($K = 45$)	100	99.7	99.7	99.4

as the p_k dataset, and ImageNet [8] as the p_{-k} dataset. We use the standard ResNet50 as the D model and use Algorithm 3 to train D models. Generated images are of resolution 256×256 .

We first demonstrate a few interesting applications of the generative approach. As discussed earlier, our approach transforms out-of-distribution data into in-distribution data by performing gradient ascent on the D model. In Figure 2 and Figure 3, by performing gradient ascent on a D model train on the CelebA-HQ dataset, we transform pixelated faces and cartoon faces into realistic human faces. Because each step of gradient ascent results in a new data sample, the generation process can be controlled by adjusting gradient ascent step size and number of steps. As a demonstration, in Figure 4 and Figure 5 we show the intermediate images produced during the process of gradient ascent.

We next show that the D model captures the target data distribution p_k reasonably well. We first sample out-of-distribution data (Figure 17) from the ImageNet (test set), and then generate new images by performing gradient ascent on D models trained on CelebA-HQ, LSUN-BEDROOM, and ImageNet-Dog dataset. Results in Figure 14, Figure 15, and Figure 16 show that the D models could generate realistic and diverse images.

Advantages and disadvantages In contrast to standard generative modeling approaches, this new generative modeling approach does not learn a fixed generator, but instead generates samples through a dynamic process of gradient ascent. This feature facilitates the implementation of certain image transformation tasks, and allows the user to take full control of the generation process. We also find the training (Algorithm 3) to be as stable as ordinary supervised training; the only failure mode (gradient ascent on D results in noisy images) that we observed is caused by λ being too large (Appendix F).

6 Conclusions and future work

In this paper we analyzed the optimal solutions of the GAT training objective and the convergence property of the training algorithm. We made a comparative analysis of the maximin formulation and minimax formulation that are respectively employed by GAT and GANs. Building on these results, we designed an incremental GAT algorithm, and evaluated it on the task of image generation and adversarial out-of-distribution detection. The good performance and training stability of the algorithm suggest that the proposed approach could serve as a new tool for content creation. Out-of-distribution detection results indicate that an OOD detection model’s robustness could be improved by training the model against an adversary equipped with large-scale, diverse OOD data.

We find that generated images are not as realistic as those produced by state-of-the-art generative models; in the future we will focus on improving the method’s generation performance by optimizing hyperparameters and model architectures. The proposed approach also has potential applications to where the GANs framework is applicable; we will look into these directions in the future.

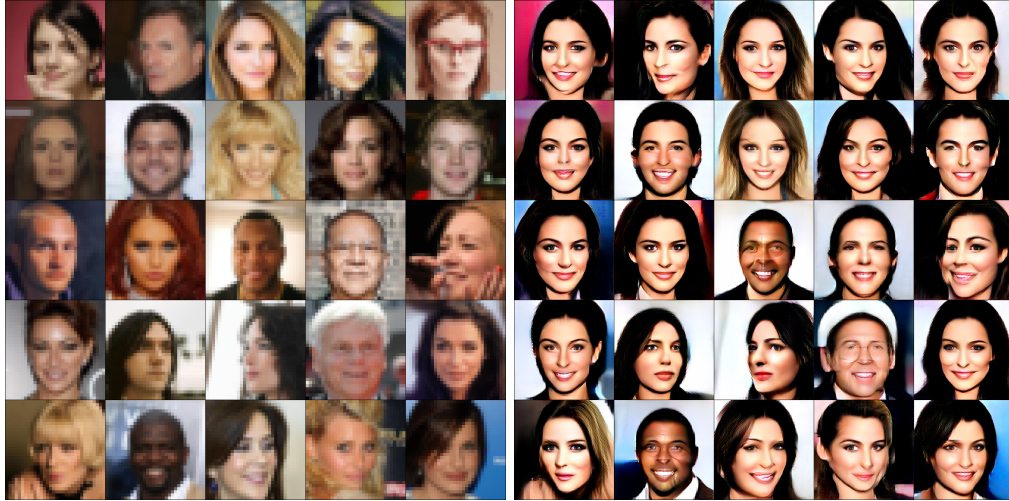


Figure 2: Transforming low-resolution faces to high-resolution faces. Image on the right subfigure were generated using the left pixelated images as starting points and performing gradient ascent on the D model trained on the CelebA-HQ dataset. The pixelated images were produced from a test split of the CelebA-HQ dataset.

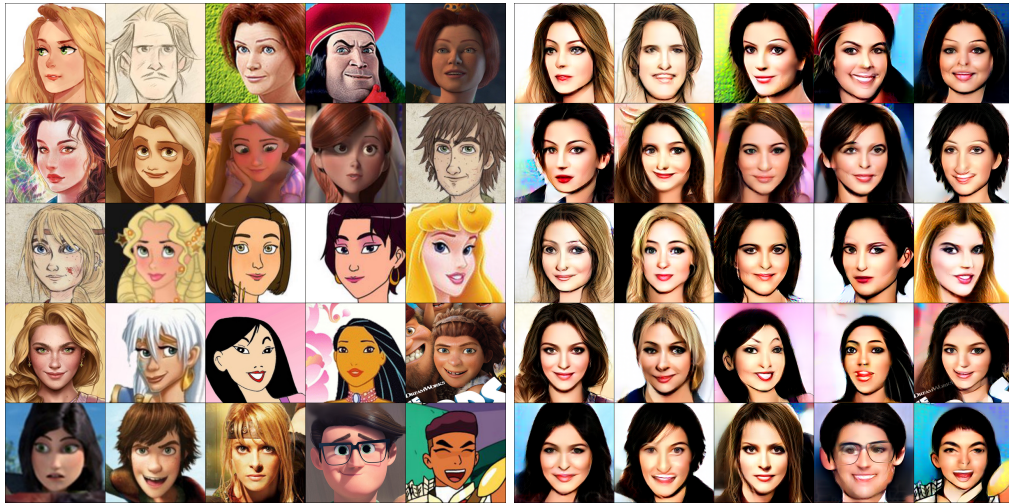


Figure 3: Transforming Cartoon faces into real faces. Image on the right subfigure were generated using the left cartoon faces as starting points and performing gradient ascent on the D model.



Figure 4: Transforming cartoon faces into bedroom images by performing gradient ascent on the D model trained on the LSUN-BEDROOM dataset.

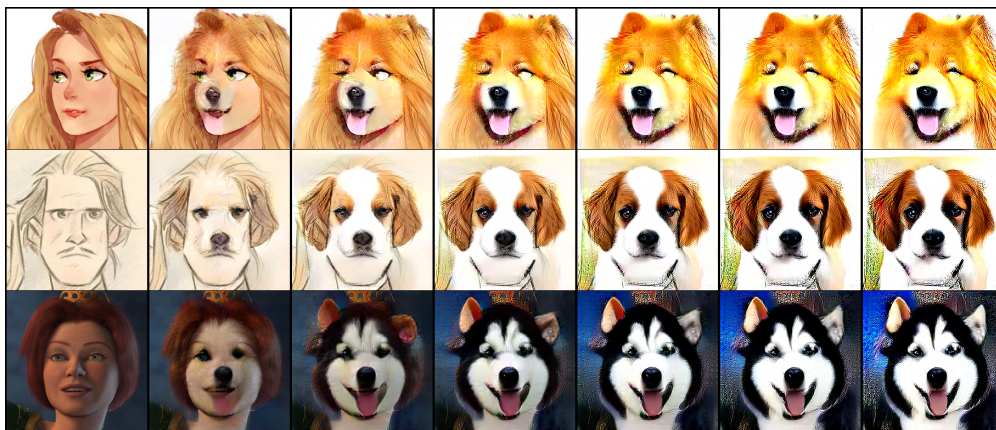


Figure 5: Transforming cartoon faces into dog faces by performing gradient ascent on the D models trained on the Image-Dog dataset.

References

- [1] Vahdat Abdelzad, Krzysztof Czarnecki, Rick Salay, Taylor Denouden, Sachin Vernekar, and Buu Phan. Detecting out-of-distribution inputs in deep neural networks using an early-layer output. *arXiv preprint arXiv:1910.10307*, 2019.
- [2] Julian Bitterwolf, Alexander Meinke, and Matthias Hein. Certifiably adversarially robust detection of out-of-distribution data. *Advances in Neural Information Processing Systems*, 33, 2020.
- [3] Stephen Boyd, Stephen P Boyd, and Lieven Vandenberghe. *Convex optimization*. Cambridge university press, 2004.
- [4] Andrew Brock, Jeff Donahue, and Karen Simonyan. Large scale gan training for high fidelity natural image synthesis. *arXiv preprint arXiv:1809.11096*, 2018.
- [5] Wenhua Chen, Yilin Shen, Hongxia Jin, and William Wang. A variational dirichlet framework for out-of-distribution detection. *arXiv preprint arXiv:1811.07308*, 2018.
- [6] Hyunsun Choi, Eric Jang, and Alexander A Alemi. Waic, but why? generative ensembles for robust anomaly detection. *arXiv preprint arXiv:1810.01392*, 2018.
- [7] Erik Daxberger and José Miguel Hernández-Lobato. Bayesian variational autoencoders for unsupervised out-of-distribution detection. *arXiv preprint arXiv:1912.05651*, 2019.
- [8] Jia Deng, Wei Dong, Richard Socher, Li-Jia Li, Kai Li, and Li Fei-Fei. Imagenet: A large-scale hierarchical image database. In *2009 IEEE conference on computer vision and pattern recognition*, pp. 248–255. Ieee, 2009.
- [9] Terrance DeVries and Graham W Taylor. Learning confidence for out-of-distribution detection in neural networks. *arXiv preprint arXiv:1802.04865*, 2018.
- [10] Laurent Dinh, Jascha Sohl-Dickstein, and Samy Bengio. Density estimation using real nvp. *arXiv preprint arXiv:1605.08803*, 2016.
- [11] Izhak Golan and Ran El-Yaniv. Deep anomaly detection using geometric transformations. In *Advances in Neural Information Processing Systems*, pp. 9758–9769, 2018.
- [12] Ian Goodfellow. Nips 2016 tutorial: Generative adversarial networks. *arXiv preprint arXiv:1701.00160*, 2016.
- [13] Ian Goodfellow, Jean Pouget-Abadie, Mehdi Mirza, Bing Xu, David Warde-Farley, Sherjil Ozair, Aaron Courville, and Yoshua Bengio. Generative adversarial nets. In *Advances in neural information processing systems*, pp. 2672–2680, 2014.
- [14] Ian Goodfellow, Yoshua Bengio, Aaron Courville, and Yoshua Bengio. *Deep learning*, volume 1. MIT press Cambridge, 2016.
- [15] Matthias Hein, Maksym Andriushchenko, and Julian Bitterwolf. Why relu networks yield high-confidence predictions far away from the training data and how to mitigate the problem. In *Proceedings of the IEEE Conference on Computer Vision and Pattern Recognition*, pp. 41–50, 2019.

- [16] Dan Hendrycks and Kevin Gimpel. A baseline for detecting misclassified and out-of-distribution examples in neural networks. *arXiv preprint arXiv:1610.02136*, 2016.
- [17] Dan Hendrycks, Mantas Mazeika, and Thomas Dietterich. Deep anomaly detection with outlier exposure. *arXiv preprint arXiv:1812.04606*, 2018.
- [18] Dan Hendrycks, Mantas Mazeika, Saurav Kadavath, and Dawn Song. Using self-supervised learning can improve model robustness and uncertainty. In *Advances in Neural Information Processing Systems*, pp. 15663–15674, 2019.
- [19] Yujia Huang, Sihui Dai, Tan Nguyen, Richard G Baraniuk, and Anima Anandkumar. Out-of-distribution detection using neural rendering generative models. *arXiv preprint arXiv:1907.04572*, 2019.
- [20] Tero Karras, Timo Aila, Samuli Laine, and Jaakko Lehtinen. Progressive growing of gans for improved quality, stability, and variation. *arXiv preprint arXiv:1710.10196*, 2017.
- [21] Tero Karras, Samuli Laine, and Timo Aila. A style-based generator architecture for generative adversarial networks. In *Proceedings of the IEEE Conference on Computer Vision and Pattern Recognition*, pp. 4401–4410, 2019.
- [22] Diederik P Kingma. Fast gradient-based inference with continuous latent variable models in auxiliary form. *arXiv preprint arXiv:1306.0733*, 2013.
- [23] Durk P Kingma and Prafulla Dhariwal. Glow: Generative flow with invertible 1x1 convolutions. In *Advances in neural information processing systems*, pp. 10215–10224, 2018.
- [24] Polina Kirichenko, Pavel Izmailov, and Andrew Gordon Wilson. Why normalizing flows fail to detect out-of-distribution data. *Advances in neural information processing systems*, 33, 2020.
- [25] Zico Kolter and Aleksander Madry. Adversarial robustness - theory and practice, 2019. URL <https://adversarial-ml-tutorial.org/>.
- [26] Jernej Kos, Ian Fischer, and Dawn Song. Adversarial examples for generative models. In *2018 IEEE security and privacy workshops (spw)*, pp. 36–42. IEEE, 2018.
- [27] Alex Krizhevsky, Geoffrey Hinton, et al. Learning multiple layers of features from tiny images. 2009.
- [28] Karol Kurach, Mario Lucic, Xiaohua Zhai, Marcin Michalski, and Sylvain Gelly. A large-scale study on regularization and normalization in gans. *arXiv preprint arXiv:1807.04720*, 2018.
- [29] Kimin Lee, Honglak Lee, Kibok Lee, and Jinwoo Shin. Training confidence-calibrated classifiers for detecting out-of-distribution samples. *arXiv preprint arXiv:1711.09325*, 2017.
- [30] Kimin Lee, Kibok Lee, Honglak Lee, and Jinwoo Shin. A simple unified framework for detecting out-of-distribution samples and adversarial attacks. In *Advances in Neural Information Processing Systems*, pp. 7167–7177, 2018.
- [31] Shiyu Liang, Yixuan Li, and Rayadurgam Srikant. Enhancing the reliability of out-of-distribution image detection in neural networks. *arXiv preprint arXiv:1706.02690*, 2017.
- [32] Weitang Liu, Xiaoyun Wang, John Owens, and Sharon Yixuan Li. Energy-based out-of-distribution detection. *Advances in Neural Information Processing Systems*, 33, 2020.

- [33] Aleksander Madry, Aleksandar Makelov, Ludwig Schmidt, Dimitris Tsipras, and Adrian Vladu. Towards deep learning models resistant to adversarial attacks. *arXiv preprint arXiv:1706.06083*, 2017.
- [34] Andrey Malinin and Mark Gales. Predictive uncertainty estimation via prior networks. In *Advances in Neural Information Processing Systems*, pp. 7047–7058, 2018.
- [35] Suvojit Manna. celeba-hq-dataset-download (github repository), 2020. URL <https://github.com/suvojit-0x55aa/celebA-HQ-dataset-download>.
- [36] Alexander Meinke and Matthias Hein. Towards neural networks that provably know when they don’t know. *arXiv preprint arXiv:1909.12180*, 2019.
- [37] Eric Nalisnick, Akihiro Matsukawa, Yee Whye Teh, Dilan Gorur, and Balaji Lakshminarayanan. Do deep generative models know what they don’t know? *arXiv preprint arXiv:1810.09136*, 2018.
- [38] Eric Nalisnick, Akihiro Matsukawa, Yee Whye Teh, and Balaji Lakshminarayanan. Detecting out-of-distribution inputs to deep generative models using a test for typicality. *arXiv preprint arXiv:1906.02994*, 5, 2019.
- [39] Yuval Netzer, Tao Wang, Adam Coates, Alessandro Bissacco, Bo Wu, and Andrew Y Ng. Reading digits in natural images with unsupervised feature learning. 2011.
- [40] J v Neumann. Zur theorie der gesellschaftsspiele. *Mathematische annalen*, 100(1):295–320, 1928.
- [41] Aaron van den Oord, Nal Kalchbrenner, and Koray Kavukcuoglu. Pixel recurrent neural networks. *arXiv preprint arXiv:1601.06759*, 2016.
- [42] F. Pedregosa, G. Varoquaux, A. Gramfort, V. Michel, B. Thirion, O. Grisel, M. Blondel, P. Prettenhofer, R. Weiss, V. Dubourg, J. Vanderplas, A. Passos, D. Cournapeau, M. Brucher, M. Perrot, and E. Duchesnay. Scikit-learn: Machine learning in Python. *Journal of Machine Learning Research*, 12:2825–2830, 2011.
- [43] Marco AF Pimentel, David A Clifton, Lei Clifton, and Lionel Tarassenko. A review of novelty detection. *Signal Processing*, 99:215–249, 2014.
- [44] Phillip Pope, Yogesh Balaji, and Soheil Feizi. Adversarial robustness of flow-based generative models. In *International Conference on Artificial Intelligence and Statistics*, pp. 3795–3805. PMLR, 2020.
- [45] Igor M Quintanilha, Roberto de ME Filho, José Lezama, Mauricio Delbracio, and Leonardo O Nunes. Detecting out-of-distribution samples using low-order deep features statistics. 2018.
- [46] Jie Ren, Peter J Liu, Emily Fertig, Jasper Snoek, Ryan Poplin, Mark Depristo, Joshua Dillon, and Balaji Lakshminarayanan. Likelihood ratios for out-of-distribution detection. In *Advances in Neural Information Processing Systems*, pp. 14707–14718, 2019.
- [47] Danilo Jimenez Rezende, Shakir Mohamed, and Daan Wierstra. Stochastic backpropagation and approximate inference in deep generative models. *arXiv preprint arXiv:1401.4082*, 2014.

- [48] Olga Russakovsky, Jia Deng, Hao Su, Jonathan Krause, Sanjeev Satheesh, Sean Ma, Zhiheng Huang, Andrej Karpathy, Aditya Khosla, Michael Bernstein, et al. Imagenet large scale visual recognition challenge. *International journal of computer vision*, 115(3):211–252, 2015.
- [49] Tim Salimans, Andrej Karpathy, Xi Chen, and Diederik P Kingma. Pixelcnn++: A pixelcnn implementation with discretized logistic mixture. *ICLR*.
- [50] Chandramouli Shama Sastry and Sageev Oore. Detecting out-of-distribution examples with in-distribution examples and gram matrices. *arXiv preprint arXiv:1912.12510*, 2019.
- [51] Vikash Sehwal, Arjun Nitin Bhagoji, Liwei Song, Chawin Sitawarin, Daniel Cullina, Mung Chiang, and Prateek Mittal. Better the devil you know: An analysis of evasion attacks using out-of-distribution adversarial examples. *arXiv preprint arXiv:1905.01726*, 2019.
- [52] Joan Serra, David Álvarez, Vicenç Gómez, Olga Slizovskaia, José F Núñez, and Jordi Luque. Input complexity and out-of-distribution detection with likelihood-based generative models. *arXiv preprint arXiv:1909.11480*, 2019.
- [53] Alireza Shafaei, Mark Schmidt, and James J Little. Does your model know the digit 6 is not a cat? a less biased evaluation of " outlier" detectors. 2018.
- [54] Gabi Shalev, Yossi Adi, and Joseph Keshet. Out-of-distribution detection using multiple semantic label representations. In *Advances in Neural Information Processing Systems*, pp. 7375–7385, 2018.
- [55] Jiaming Song, Yang Song, and Stefano Ermon. Unsupervised out-of-distribution detection with batch normalization. *arXiv preprint arXiv:1910.09115*, 2019.
- [56] Christian Szegedy, Wojciech Zaremba, Ilya Sutskever, Joan Bruna, Dumitru Erhan, Ian Goodfellow, and Rob Fergus. Intriguing properties of neural networks. *arXiv preprint arXiv:1312.6199*, 2013.
- [57] Antonio Torralba, Rob Fergus, and William T Freeman. 80 million tiny images: A large data set for nonparametric object and scene recognition. *IEEE transactions on pattern analysis and machine intelligence*, 30(11):1958–1970, 2008.
- [58] Florian Tramèr, Nicholas Carlini, Wieland Brendel, and Aleksander Madry. On adaptive attacks to adversarial example defenses. *arXiv preprint arXiv:2002.08347*, 2020.
- [59] Dimitris Tsipras, Shibani Santurkar, Logan Engstrom, Alexander Turner, and Aleksander Madry. Robustness may be at odds with accuracy. *arXiv preprint arXiv:1805.12152*, 2018.
- [60] Sachin Vernekar, Ashish Gaurav, Vahdat Abdelzad, Taylor Denouden, Rick Salay, and Krzysztof Czarnecki. Out-of-distribution detection in classifiers via generation. *arXiv preprint arXiv:1910.04241*, 2019.
- [61] Xuwang Yin, Soheil Kolouri, and Gustavo K Rohde. Gat: Generative adversarial training for adversarial example detection and robust classification. In *International Conference on Learning Representations*, 2020. URL <https://openreview.net/forum?id=SJeQEp4YDH>.
- [62] Fisher Yu, Ari Seff, Yinda Zhang, Shuran Song, Thomas Funkhouser, and Jianxiong Xiao. Lsun: Construction of a large-scale image dataset using deep learning with humans in the loop. *arXiv preprint arXiv:1506.03365*, 2015.

- [63] Qing Yu and Kiyoharu Aizawa. Unsupervised out-of-distribution detection by maximum classifier discrepancy. In *Proceedings of the IEEE International Conference on Computer Vision*, pp. 9518–9526, 2019.
- [64] Han Zhang, Tao Xu, Hongsheng Li, Shaoting Zhang, Xiaogang Wang, Xiaolei Huang, and Dimitris N Metaxas. Stackgan++: Realistic image synthesis with stacked generative adversarial networks. *IEEE transactions on pattern analysis and machine intelligence*, 41(8):1947–1962, 2018.

A GAT training algorithm

Algorithm 4 GAT Single-Class Detector Training Algorithm

- 1: Sample minibatch of m samples $\{x_1^k, \dots, x_m^k\}$ from p_k , and m samples $\{x_1^{-k}, \dots, x_m^{-k}\}$ from p_{-k} .
 - 2: Compute adversarial examples $\{x'_1, \dots, x'_m\}$ by solving $\max_{x' \in \mathbb{B}(x, \epsilon)} D(x')$ for each x_i^{-k} .
 - 3: Train the detector by minimizing $\frac{1}{m} \sum_{i=1}^m [-\log D(x_i^k) - \log(1 - D(x'_i))]$ (single step).
 - 4: Return to step 1.
-

B related work on out-of-distribution detection

Out-of-distribution (OOD) detection, also known as novelty detection, or anomaly detection, deals with the problem of identifying novel, or unusual, data from within a dataset. OOD detection has gained much research attention due to its practical importance in safety-critical applications and changeling nature. A comprehensive review of classical OOD detection methods can be found at [43].

A recent surge of research interests in this topic is due to the emergence of deep generative models. Such models (specifically explicit density models [12]) estimate the generative probability density function of the data, and should serve as an ideal candidate for OOD detection. However, it was observed [24, 37, 53, 17] that several state-of-the-art deep generative models, including Glow [23], PixelCNN [41], PixelCNN++ [49], VAEs [22, 47], and RealNVP flow model [10] tend to assign higher likelihood to OOD inputs than they do to in-distribution inputs. Despite this challenge, several recent works [46, 6, 38, 24, 52, 55, 19, 7] investigated the issue and successfully applied deep generative models to OOD detection.

There is also a plethora of OOD detection methods [16, 30, 31, 50, 45, 1, 5, 34] that make use of statistics computed from the predictions or intermediate activations of standard classifiers train on in-distribution data. To name a few, [30] fit class conditional Gaussian distributions using multiple levels of activations of the classifier, and use Mahalanobis distance to compute confidence scores to identify OOD inputs. The ODIN method [31] improves the effectiveness of a softmax score based detection approach by using temperature scaling and adding small perturbations to the input. [50] make use of Gram matrices computed from the classifier’s intermediate activations to identify OOD inputs.

Another branch of work utilize various alternative training strategies [32, 29, 17, 18, 9, 54, 60, 63, 11]. A notable example is the Outlier Exposure (OE) method [17]. OE works by training the OOD detector against a large, diverse out-of-distribution dataset, and has been widely adopted as a baseline method.

While methods based on generative models and standard classifiers yield high performances on naturally-occurring OOD inputs, several such methods have been shown [36, 2] to be vulnerable to adversarial manipulation of the OOD inputs. This should come as no surprise as both generative models and standard classifiers themselves are vulnerable to adversarial attacks [26, 56, 44]. Given the above limitation of current approaches, a recent trend considers the worst-case scenario for OOD detection [15, 51, 36, 2]. The Adversarial Confidence Enhanced Training (ACET) method proposed by [15] use adversarial training [33] on OOD inputs to improve detection robustness. [36] uses a density estimator to provide guarantees on the maximal confidence around L^2 ball for uniform noise. [2] use interval-bound-propagation (IBP) to certificate worst case guarantees for general OOD inputs under a L^∞ threat model. In the same spirit as [15], our detection method employs adversarial training on OOD inputs to induce robustness. The difference is that our method uses the GAT

objective with a optimal solution which naturally deals with adversarial OOD inputs, while the optimal solution of the objective used by [15], which is essentially a multiple class classification objective with an extra term on OOD inputs, is unclear.

C Mathematical analysis of optimal solutions of the maximin problem

For the convenience of analysis, instead of using ϵ -balls imposed on individual data samples, we use the notion of a common perturbation space: The perturbation space \mathcal{S} is a subspace of the data space \mathcal{X} , and allows mass of p_{-k} to be moved to any location in \mathcal{S} . A new distribution p_t can be obtained by transporting the mass of p_{-k} to appropriate locations in \mathcal{S} , via a transformation function $T : \mathcal{S} \rightarrow \mathcal{S}$. Utilizing the technique of random variable transformation, we can write the density function of p_t as a function of p_{-k} : $p_t(y) = \int_{\mathcal{S}} p_{-k}(x) \delta(y - T(x)) dx$. Figure 6 left panel is a schematic illustration of this phenomenon. Let $\mathcal{M}_+^1(\mathcal{S})$ be the set of distributions attainable by applying such transformations to the support of p_{-k} .

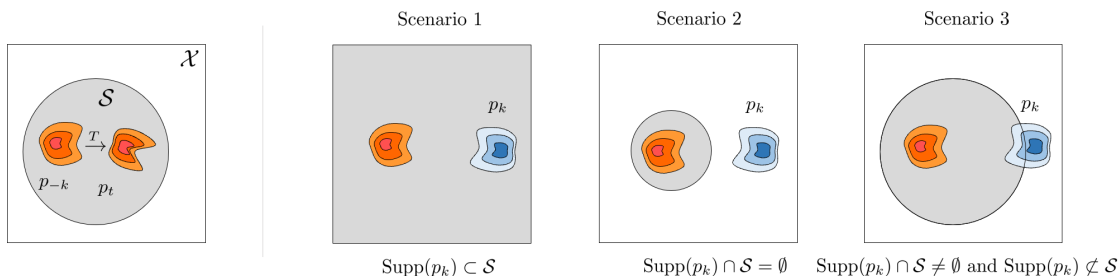


Figure 6: Left panel: a distribution p_t is obtained by applying a transformation T to the support of p_{-k} . Right panel: three scenarios to consider when analyzing problem 5. Red distribution represents p_{-k} and blue distribution represents p_k . The data space \mathcal{X} is represented by the whole space inside the square, and the perturbation space \mathcal{S} is represented by the gray area.

Table 3: Optimal solutions for the three scenarios in Figure 6

Scenario	Optimal solution (D^*, p_t^*)
Supp(p_k) \subset \mathcal{S}	D^* outputs $\frac{1}{2}$ for Supp(p_k) and $\leq \frac{1}{2}$ for $\mathcal{S} \setminus \text{Supp}(p_k)$; p_t^* has its mass distributed to locations where D^* outputs $\frac{1}{2}$.
Supp(p_k) \cap \mathcal{S} = \emptyset	D^* outputs 1 for Supp(p_k) and 0 for \mathcal{S} ; p_t^* can be an arbitrary distribution in $\mathcal{M}_+^1(\mathcal{S})$.
Supp(p_k) \cap \mathcal{S} \neq \emptyset , and Supp(p_k) $\not\subset$ \mathcal{S}	For Supp(p_k) outside \mathcal{S} , D^* outputs 1, for Supp(p_k) inside \mathcal{S} , D^* outputs $\alpha = \frac{\int_{\mathcal{S}} p_k}{\int_{\mathcal{S}} p_t^* + \int_{\mathcal{S}} p_k}$ (by definition, $\int_{\mathcal{S}} p_t^* = 1$), and for other locations inside \mathcal{S} , D^* outputs $\leq \alpha$; p_t^* has its mass distributed to locations where D^* outputs α .

Mathematical analysis Recall that the support of p_t can be any subset of the perturbation space \mathcal{S} and that $U(D, p_t) = \int p_k(x) \log D(x) dx + \int p_t(x) \log(1 - D(x)) dx$. For convenience, we define the contour set inside \mathcal{S} of D at α as $C_\alpha^D := \{x \in \mathcal{S} : D(x) = \alpha\}$, the region of Supp(p_k) that is outside of \mathcal{S} as $\Omega_{ko} := \text{Supp}(p_k) \setminus \mathcal{S}$ and the region of Supp(p_k) that is in \mathcal{S} as $\Omega_{ki} := \text{Supp}(p_k) \cap \mathcal{S}$. Note that $\text{Supp}(p_k) = \Omega_{ko} \cup \Omega_{ki}$. For a fixed D and let $\alpha_o = \max_{\Omega_{ko}} D$ and $\alpha_S = \max_{\mathcal{S}} D$. It is easy to check that U is minimized when Supp(p_t) lies in the contour set $C_{\alpha_S}^D$. Let p_t^* be a distribution

such that $\text{Supp}(p_t^*) \subset C_{\alpha_S}^D$. By direct computation we have that

$$\begin{aligned} U(D, p_t^*) &= \int_{\Omega_{k_o}} p_k(x) \log D(x) dx + \int_{\Omega_{k_i}} p_k(x) \log D(x) dx + \log(1 - \alpha_S) \\ &\leq \left(\int_{\Omega_{k_o}} p_k \right) (\log \alpha_k) + \left(\int_{\Omega_{k_i}} p_k \right) (\log \alpha_S) + \log(1 - \alpha_S) \\ &\leq 0 + \beta_{ki} \log \frac{\beta_{ki}}{1 + \beta_{ki}} + \log \frac{1}{1 + \beta_{ki}}, \end{aligned}$$

where $\beta_\epsilon = \int_{\Omega_{k_i}} p_k$. Note here we have used the fact the the function $f(y) = a \log y + b \log(1 - y)$ achieves its maximum at $y = \frac{a}{a+b}$. It is not difficult to see that the above inequality becomes an equality when

$$D(x) = \begin{cases} \alpha_k & x \in \Omega_{k_o} \\ \alpha_S & x \in \Omega_{k_i} \\ \leq \alpha_S & x \in \mathcal{S} \setminus \text{Supp}(p_k) \end{cases}, \quad (6)$$

where $\alpha_k = 1$ and $\alpha_S = \frac{\beta_{ki}}{1 + \beta_{ki}}$. Note that D does not need to be defined outside $\mathcal{S} \cup \text{Supp}(p_k)$.

Scenario 1 Here we deal with the case when ϵ is large enough such that $\text{Supp}(p_k) \subset \mathcal{S}$, in which case $\Omega_{k_o} = \emptyset$, $\Omega_{k_i} = \text{Supp}(p_k)$ and $\alpha_S = \frac{1}{2}$. Hence by the above analysis one can check that U achieves its optimum when $D \equiv \alpha_S = \frac{1}{2}$ on $\text{Supp}(p_k)$ and $D \leq \frac{1}{2}$ on $\mathcal{S} \setminus \text{Supp}(p_k)$. In summary, the maximin problem achieves its optimum when D outputs $\frac{1}{2}$ on the support of p_k and values less or equal to $\frac{1}{2}$ on samples outside the support of p_k but in \mathcal{S} .

Scenario 2 Here we deal with the case when ϵ is small enough such that the $\mathcal{S} \cap \text{Supp}(p_k) = \emptyset$, in which case $\Omega_{k_o} = \text{Supp}(p_k)$, $\Omega_{k_i} = \emptyset$ and $\alpha_S = 0$. Hence U achieves its optimum when $D \equiv 1$ on $\text{Supp}(p_k)$ and $D \equiv 0$ on \mathcal{S} . In summary, the maximin problem achieves its optimum when D outputs 1 on the support of p_k and zero on the the perturbation space \mathcal{S} .

Scenario 3 Here we deal with the case when $\mathcal{S} \cap \text{Supp}(p_k) \neq \emptyset$ and $\text{Supp}(p_k) \not\subset \mathcal{S}$. In summary, the maximin problem achieves its optimum when D outputs 1 on the set of samples inside the support of p_k but outside of the perturbation space \mathcal{S} and $\frac{\beta_{ki}}{1 + \beta_{ki}}$ on the set of samples that are in the intersection of the support of p_k and \mathcal{S} and values less or equal to $\frac{\beta_{ki}}{1 + \beta_{ki}}$ on \mathcal{S} .

Remark The first two cases can be seen as the special cases of the third one.

Additional discussion on Scenario 2 In robust machine learning literature, it's common to consider a very small value for ϵ . For instance, one of the most commonly used limit for training L^∞ robust models is $\epsilon = 8/255$ (L^∞ norm). A perturbation space characterized by a small limit can be thought as a semantic-preserving space: translating a sample inside the space doesn't change the sample's underlying label/class membership. A small perturbation limit corresponds to scenario 2, which is also the focus of Yin et al. [61]. We can define robust models as models that output consistent predictions for inputs under semantic-preserving transformations. In this sense, the optimal D for scenario 2 is a robust detector, as it always outputs 0 for the perturbation space. However, the limitation of training against a small ϵ is obvious: because optimal D 's outputs outside $\mathcal{S} \cup \text{Supp}(p_k)$ are unspecified, any semantic-preserving operation that has a perturbation that goes beyond \mathcal{S} can result in a high D output, thereby fools the detection. The above analysis suggests that for predictive models based on the generative adversarial training method, their robustness can be improved by training against a larger perturbation space.

D Algorithm 1 convergence

D.1 The effects of alternating optimization

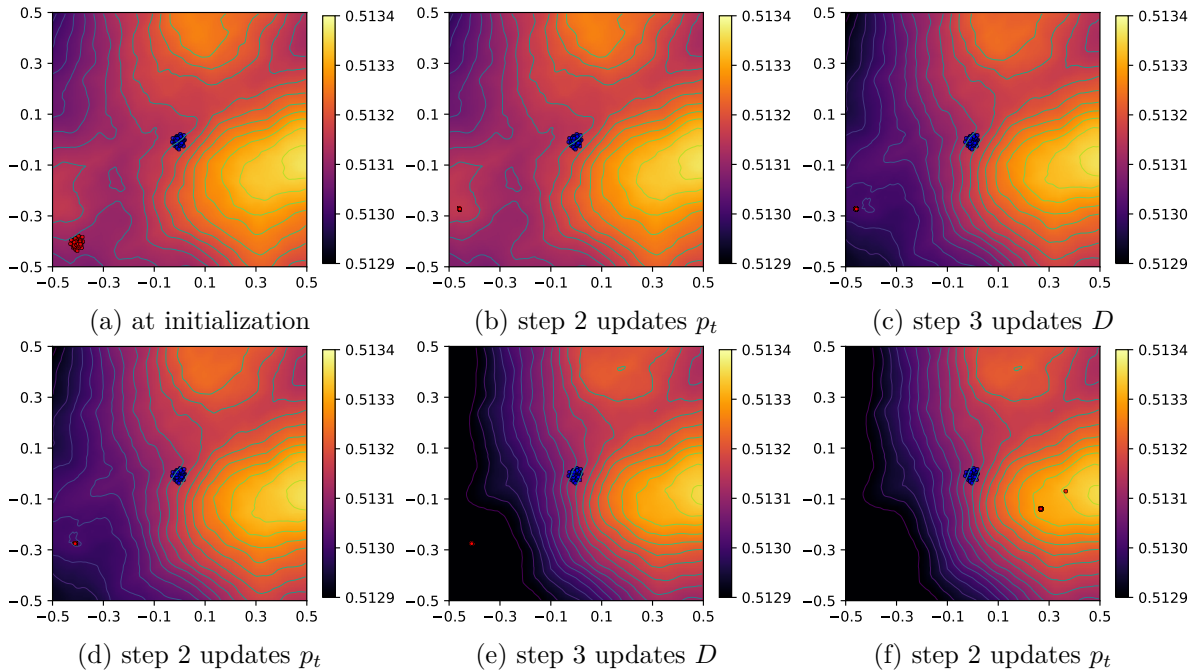


Figure 7: The results of p_t and D in the first few iterations of a 2D simulation of Algorithm 1. Step 2 solves the inner minimization, causes support of p_t (red points) to be concentrated in local maxima points. Step 3 update D by increasing its outputs on the support of p_k and decreasing its outputs on the support of p_t , causes local maxima to be suppressed.

D.2 More 2D simulation results

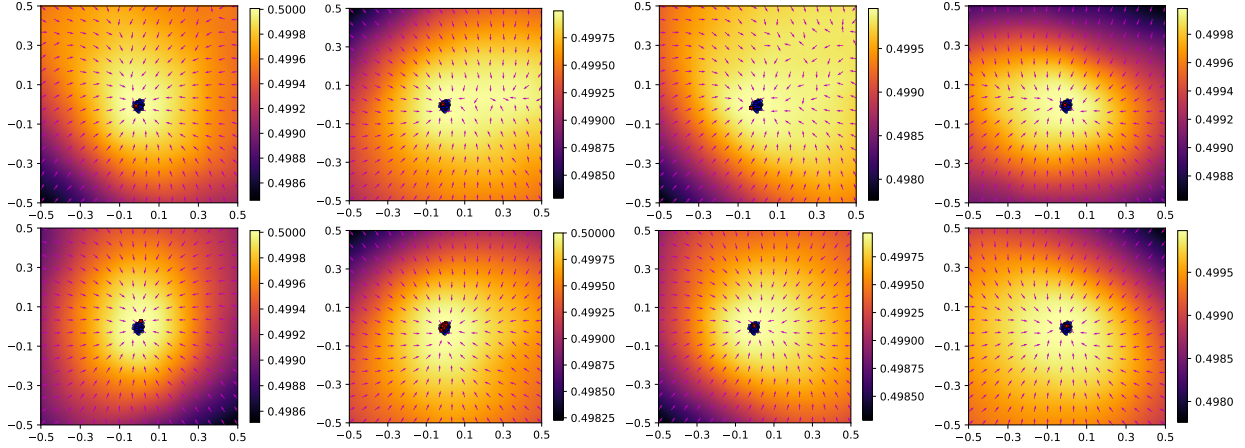


Figure 8: Solutions obtained by the *maximin* problem solver (Algorithm 1) with different initializations of D . First row are results when p_{-k} is at bottom left (Figure 1(a)), and second row are results when p_{-k} are uniform distributions.

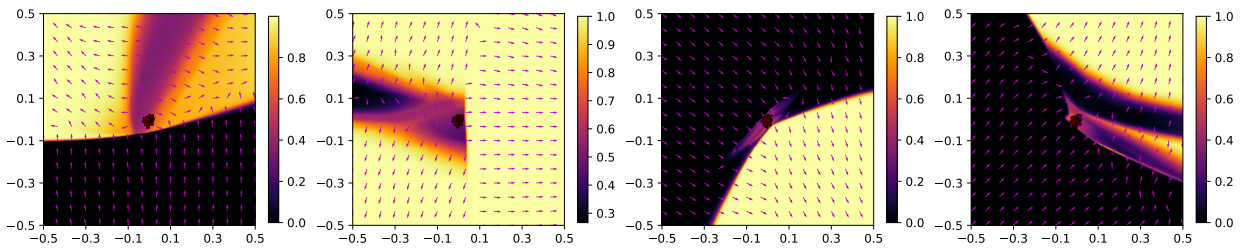


Figure 9: Solutions obtained by the *minimax* problem solver (Algorithm 2) with different initializations of D . Note that in all cases p_t (red distribution) matches p_k (blue distribution), but D has unpredictable outputs on $\mathcal{X} \setminus \text{Supp}(p_k)$. The initial position of the red distribution is in bottom left corner (see Figure 7(a)).

E Ablation Study

E.1 Effects of incremental training

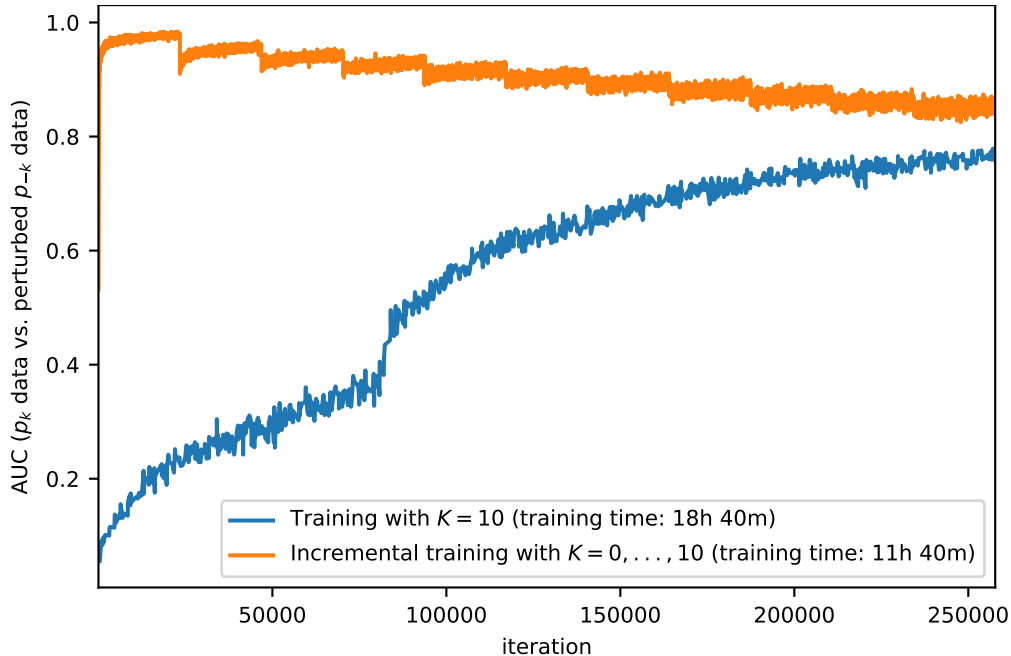


Figure 10: AUROC curves of two training schemes (p_k is CIFAR-10 and p_{-k} is the Tiny Images dataset). In the incremental scheme, the training follows Algorithm 3 and uses an increasing sequence of number of steps ($K = 0, \dots, 10$), while in the other scheme, the training uses a fixed number of steps of 10 ($K = 10$). These two schemes are trained with the same number of iterations. The AUROC values are computed using D outputs on pairs of p_k data (a batch) and perturbed p_{-k} data (a batch). A model with a high AUROC value separates these two types of data better.

E.2 Uniform noise as the p_{-k} dataset

In this ablation study, we use CIFAR-10 class 0 data as the target data distribution dataset p_k , and train the D model using uniform noise as the p_{-k} dataset. It is observed in Table 4 and 5 that when p_{-k} is uniform noise, the D models only developed capability for identifying uniform noise and Gaussian noise as OOD inputs. This result seems to contradict our mathematical analysis which states that with a uniform distribution as p_{-k} , a D function useful for detecting any kind of OOD inputs could be obtained. According to the manifold hypothesis, real image data lie on lower-dimensional manifolds embedded within the high-dimensional space; real image samples are close to each other in terms of geodesic distance. Uniform noise, on the other hand, is distributed in the entire space, and may require much larger perturbations to reach real data. As a result, uniform noise is much less data efficient than real data for training OOD detection models, and a much larger number of inner iterations and K value in Algorithm 3 may be needed to reach a satisfying detection performance.

Table 4: OOD detection performance (AUROC scores) of $K = 0$ model on CIFAR-10 class 0 data ($p_k = \text{CIFAR-10 class 0}$, and $p_{-k} = \text{uniform noise}$).

ϵ -test	Gaussian noise	Uniform noise	ImageNet	Bedroom	SVHN	CelebAHQ	CIFAR100	mean
0.0	1.0000	1.0000	0.5859	0.5791	0.5801	0.5235	0.5499	0.6884
1.0	1.0000	1.0000	0.5161	0.5028	0.5141	0.4510	0.4816	0.6379

Table 5: OOD detection performance (AUROC scores) of $K = 15$ model on CIFAR-10 class 0 data. ($p_k = \text{CIFAR-10 class 0}$, and $p_{-k} = \text{uniform noise}$).

ϵ -test	Gaussian noise	Uniform noise	ImageNet	Bedroom	SVHN	CelebAHQ	CIFAR100	mean
0.0	1.0000	1.0000	0.5772	0.5760	0.5711	0.5139	0.5435	0.6831
1.0	1.0000	1.0000	0.5063	0.4984	0.5043	0.4406	0.4738	0.6319

F Failure mode diagnosis

We observe that in Algorithm 3, if λ is set to a too large value, the algorithm fails to learn a D that is useful for image generation. In this section we discuss the training dynamics of the case of an appropriate λ value and the case of λ being too large.

λ is small enough In Algorithm 3 as we increase K , p_t gradually converges to p_k . In this process it becomes increasingly difficult for the D model to differentiate these two distributions. This phenomenon can be observed in Figure 11 : the training loss (binary cross-entropy loss) of the D model becomes larger and larger (left subfigure), and eventually these two distributions become indistinguishable (AUROC ≈ 0.5 , middle subfigure). From the right subfigure we can see that D 's performance on p_{-k} vs. p_k is also affected by the increase in K value.

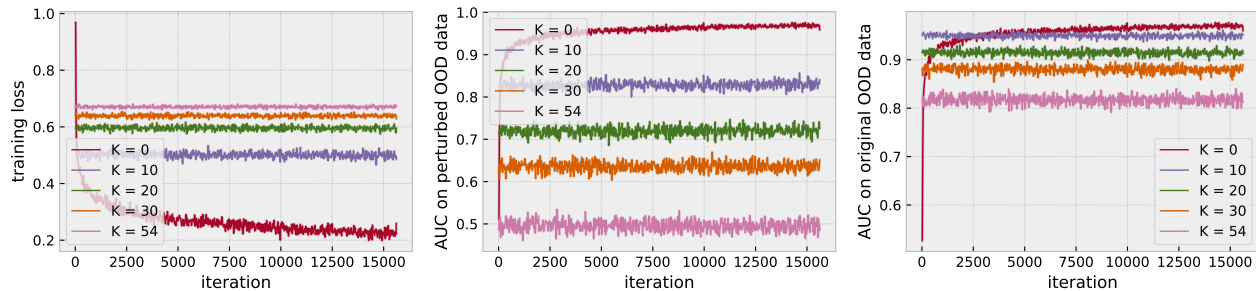


Figure 11: CIFAR-10 training curves of $\lambda = 0.1$. Left: training loss curves, middle: AUROC curves (p_t vs. p_k), and right: AUC curves (p_{-k} vs. p_k).

λ is too large The failure mode caused by λ being too large is easy to identify (Figure 12): the training loss quickly decreases to 0 as K increases (left subfigure), p_t and p_k become perfectly separable (middle subfigure), and D model becomes unable to separate p_{-k} from p_k (right subfigure).

In general, with a small enough λ value, an increase of sample quality could be expected after model is trained with a larger K . This is the case when λ is 0.1, but not when it is 0.6 (Figure 13).

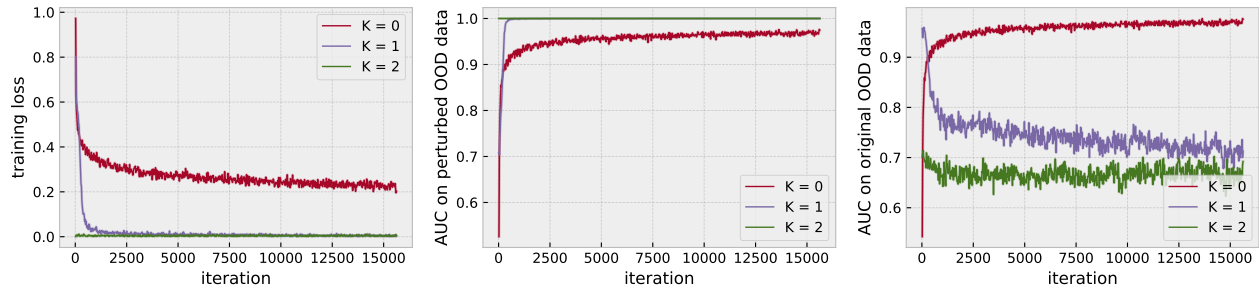


Figure 12: CIFAR-10 training curves of a failed training instance ($\lambda = 0.6$).



Figure 13: Generated samples after training with an increasing sequence of K values ($K = 0, 1, 2$). Sample quality improved when $\lambda = 0.1$, but didn't when $\lambda = 0.6$.

G Extended adversarial OOD detection results

Table 6: The performance (AUROC scores) of CIFAR-10 $K = 5$ model (the in-distribution dataset is CIFAR-10) under attacks of different configurations. Following [2] we used 1000 samples for both in-distribution data and OOD data. Similarly, we used 5 random restarts to enhance the default attack, but the performance decrease is negligible.

PGD attack steps, step size	OOD dataset (with an L^∞ perturbation of $\epsilon = 0.01$)			
	Uniform Noise	Gaussian Noise	SVHN	CIFAR-100
100, 0.002 (default for Table 1)	98.69	99.32	91.48	82.41
100, 0.002 (5 random restarts)	98.69	99.31	91.45	82.39
500, 0.002	98.69	99.31	91.47	82.40
500, 0.005	98.70	99.32	91.48	82.43
500, 0.01	98.71	99.39	91.57	82.61
1000, 0.001	98.69	99.31	91.47	82.40

Table 7: The performance (AUROC scores) of SVHN $K = 45$ model (the in-distribution dataset is SVHN) under attacks of different configurations. Following [2] we used 1000 samples for both in-distribution data and OOD data. Similarly, we used 5 random restarts to enhance the default attack, but the performance decrease is negligible.

PGD attack steps, step size	OOD dataset (with an L^∞ perturbation of $\epsilon = 0.03$)			
	Uniform Noise	Gaussian Noise	CIFAR-10	CIFAR-100
500, 0.002	100	99.84	99.78	99.53
100, 0.005	100	99.85	99.78	99.54
100, 0.005 (5 random restarts)	100	99.85	99.78	99.54
500, 0.005	100	99.85	99.78	99.54
500, 0.01	100	99.86	99.79	99.55
1000, 0.001	100	99.84	99.78	99.53

Table 8: Standard OOD detection performances (AUROC scores) when the in-distribution dataset is CIFAR-10 and OOD samples are not perturbed. Performance data is collected from referenced papers in the table; when there is a discrepancy we use the best reported result. Details about the iSUN, LSUN (resize), and TinyImageNet (resize) datasets can be found at [31].

Method	OOD dataset (no perturbation)						
	Uniform	Gaussian	SVHN	CIFAR-100	iSUN	LSUN(resize)	TinyImageNet (resize)
Softmax [16]	96.5	97.5	89.9	86.4	91.0	91.0	91.0
ODIN [31]	99	100	96.7	87.5	94.0	94.1	94.0
Mahalanobis [30]	100	N/A	99.1	88.2	99.5	99.7	99.5
OE [17]	98.7	99.3	98.8	95.3	98.5	98.94	N/A
Gram Matrices [50]	N/A	100	99.5	79.0	99.8	99.9	99.7
Energy-based [32]	N/A	N/A	99.4	N/A	99.33	99.39	N/A
Likelihood ratios [46]	N/A	N/A	88.8	N/A	N/A	N/A	N/A
WAIC [6]	100	100	100	N/A	N/A	N/A	95.6
CCU [36]	100	N/A	97.1	93.0	N/A	N/A	N/A
ACET [15]	99.7	N/A	92.4	90.7	N/A	N/A	N/A
GOOD [2]	99.5	N/A	97.1	92.9	N/A	N/A	N/A
Ours ($K = 0$)	99.5	99.8	99.6	94.1	99.5	99.5	98.7
Ours ($K = 5$)	99.6	99.9	97.4	91.5	98.5	98.9	96.2

H 256×256 resolution generation



Figure 14: Uncurated 256×256 generation results in the CelebA-HQ dataset.

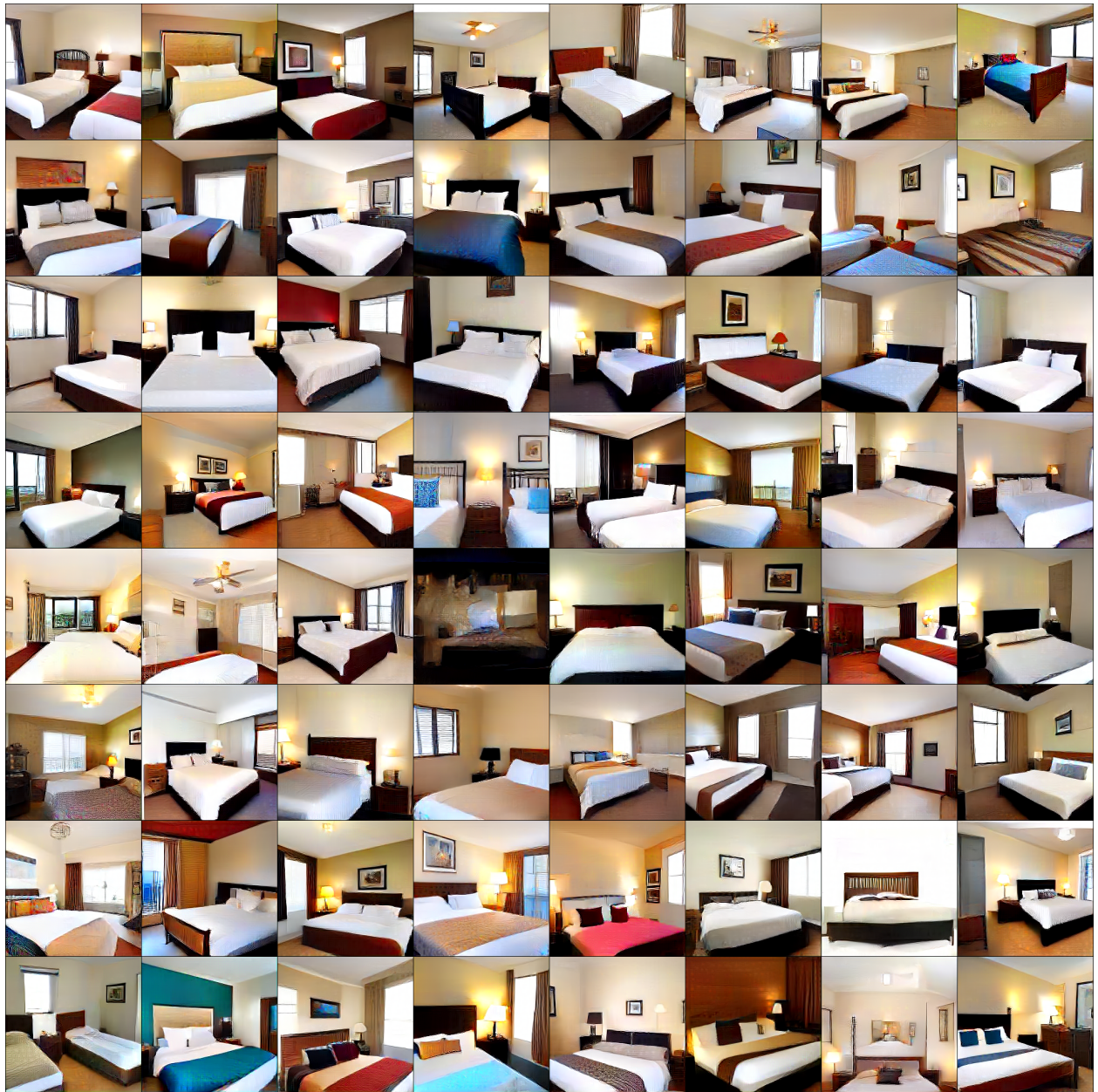


Figure 15: Uncurated 256×256 generation results in the Bedroom256 dataset.



Figure 16: Uncurated 256×256 generation results in the ImageNet-Dog dataset.

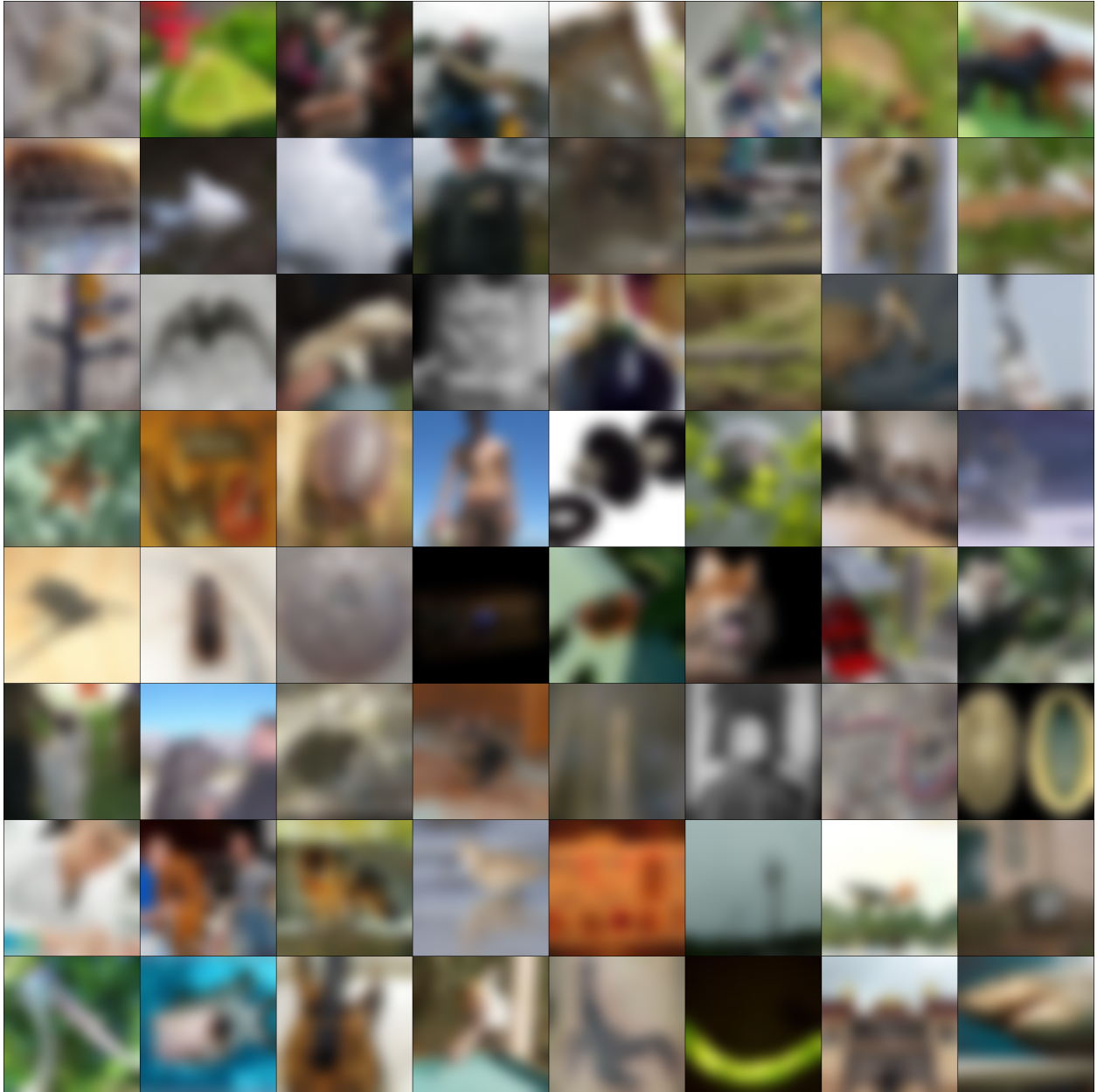


Figure 17: Out-of-distribution data used to generate images in Figure 14, Figure 15, and Figure 16. The data is produced by first sampling from ImageNet test set and then applying Gaussian blur to sampled images.